Electronic Supplementary Material (ESI) for Chemical Communications

Supporting Online Material for
Small sized perylene-bisimide assemblies controlled by both cooperative and anti-cooperative assembly processes

Rob van der Weegen, Peter A. Korevaar, Panayiotis Voudouris, Ilja K. Voets, Tom F.A. de Greef, Jef A.J.M. Vekemans and E.W. Meijer*

Institute for Complex Molecular Systems and Laboratory of Macromolecular and Organic Chemistry,, Eindhoven University of Technology, P.O. Box 513, 5600 MB Eindhoven, The Netherlands. E-mail: e.w.meijer@tue.nl; Fax: +31 (0)40 2451036; Tel: +31 (0)40 2473101

Contents

Experimental Details

Materials

Unless specifically mentioned, reagents and solvents were obtained from commercial suppliers and used without further purification. All solvents were of AR quality. Deuterated chloroform for NMR analyses was provided with TMS as a 0 ppm reference. The methylcyclohexane used in all spectroscopic experiments was of spectroscopic grade. Column chromatography was performed on a Biotage Isolera One using SNAP KP-sil columns and solvent gradients. All reactions were performed under an atmosphere of dry argon unless stated otherwise

Instrumentation

^{1}H-NMR and ^{13}C-NMR spectra were recorded on a Varian Mercury Vx 400 MHz instrument (100 MHz for ^{13}C) and all chemical shifts are reported in parts per million relative to tetramethylsilane (TMS). MALDI-ToF MS analyses were performed in reflector mode on a PerSeptive Biosystems Voyager-DE Pro using α-cyano-4-hydroxycinnamic acid (CHCA) and 2-[(2E)-3-(4-tert-butylphenyl)-2-methylprop-2-enylidene]manolnitrile (DCTB) as matrices. Ultraviolet-Visible (UV-Vis) absorbance spectra were recorded on a Jasco V-650 UV-Vis spectrometer with a Jasco ETCR-762 temperature controller. Solid state infrared (IR) spectra were recorded on a Perkin Elmer Spectrum One spectrometer equipped with a ATR universal sampler accessory and in dilute solution using 1 mm NaCl cells.

The small-angle X-ray scattering (SAXS) experiments were performed at the cSAXS beamline at the Swiss Light Source (SLS) at the Paul Scherrer Institute. The samples were filled in 1 mm diameter quartz capillaries with a wall thickness of 0.01 mm (Hilgenberg) and maintained at a temperature of 20±1°C. An X-ray energy of 12.4 keV corresponding to a wavelength, λ, of 0.1 nm and one sample-to-detector distance of 2.17 m were used, to cover a range of 0.3 $nm^{-1} \leq q \leq 2.5\ nm^{-1}$ with the magnitude of the scattering wave vector, q, given by $q = \frac{4\pi}{\lambda}\sin\left(\frac{\theta}{2}\right)$ and the scattering angle, θ. The scattering patterns were recorded on a PSI-developed Pilatus 2 M detector operating in single-photon counting mode. The 2D images were azimuthally integrated and corrected for background scattering according to established procedures provided by the PSI. The q-scale was calibrated by a measurement of silver behenate. The SASfit software package was used for data analysis with a form factor for monodisperse rigid cylinders.[1] The monomer concentration of 1 mM was low enough to safely neglect interactions between the supramolecular self-assemblies, such that the structure factor $S(q) \sim 1$.

Static light scattering (SLS) is a widely used technique for the characterization of particles in solution. The absorption of light, though, requires special precautions in order to avoid laser-induced motions of the particles, such as induced flow, which would disturb the measured signal. Care was taken to minimize the induced thermal effects, in particular to suppress the thermal lensing as observed through the projection of the transmitted beam. To control the effectiveness of the method, measurements were conducted at different laser wavelengths (740 nm, 633 nm and 532 nm) and powers and the invariance of the relaxation functions to power increase was checked. Scattered intensity was normalized to the toluene intensity. Static and dynamic light scattering experiments were conducted on FORTH/IESL Greece using an ALV-5000 commercial set-up allowing polarized scattering measurements. A He-Ne 633 nm and 20 mW power was used as the light source. The dispersions were contained in dust-free 10 mm tubes. Static light scattering measurements were obtained by averaging the intensity at each angle, over 5 to 10s and the scattering wave vector, $q = (4\pi n/\lambda)\sin(\vartheta/2)$ with n being the

refractive index of the medium and ϑ the scattering angle, was varied in a broad range between 0.007-0.028 nm^{-1}.

Synthesis

Asymmetric PBI **1** was synthesized according to Scheme 1. Perylene monoimide monoanhydride **3** and aniline **4** were synthesized according to literature procedures.[2,3,4] Condensation of aniline **4** with **3** using $Zn(OAc)_2$ as a catalyst in quinoline resulted in the formation of PBI **1**, which was fully characterized by NMR and mass spectroscopy.

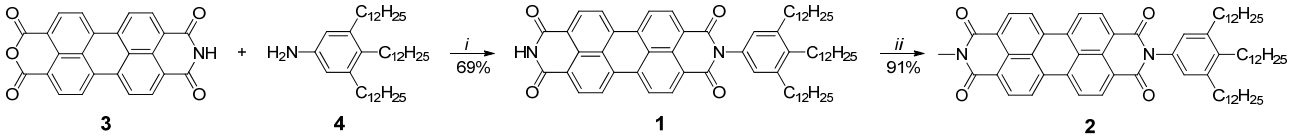

Scheme 1: Synthetic route towards PBIs **1** and **2**. Reagents and conditions: i) $Zn(OAc)_2$, quinoline, 180 ^oC; ii) MeI, K_2CO_3, DMF, RT.

N-3,4,5-tridodecylphenyl-perylene-3,4:9,10-tetracarboxylic acid bisimide **1**

Perylenetetracarboxylic acid-3,4-anhydride-9,10-imide (130 mg, 0.33 mmol), 3,4,5-tridodecylaniline (300 mg, 0.46 mmol), and $Zn(OAc)_2$ (73 mg, 0.33 mmol) were mixed in quinolone (15 mL). The mixture was stirred at 180 ^oC for 2 hour under argon atmosphere, resulting in a dark red/brown mixture. After cooling to room temperature the solution was poured into methanol (100 mL), resulting in a dark red precipitate. Remaining quinoline solvent was removed by repetitive precipitations from chloroform in methanol. The crude product was purified by silica gel column chromatography using first chloroform as eluent to remove the bisimide side-product and then 5% acetic acid in chloroform (R_f = 0.55). Acetic acid was neutralized by basic extraction with 1 M NaOH from the chloroform solution. The organic phase was dried over $MgSO_4$ and evaporated in *vacuo* to yield the product as a red solid (90 mg, 35% yield). ^{1}H-NMR ($CDCl_3$) δ = 8.73 (d, 2H, PBI), 8.67 (d, 2H, PBI), 8.63 (d, 2H, PBI), 8.61 (d, 2H, PBI), 8.57 (b, 1H, NH), 6.98 (s, 2H, benzylic), 2.66 (t, 6H, CH_2), 1.7-1.2 (mm, 60H, aliphatic), 0.92-0.82 (m, 9H, CH_3). ^{13}C-NMR ($CDCl_3$) δ = 163.5, 162.9, 142.2, 139.4, 135.3, 134.4, 132.1, 131.7, 131.2, 130.6, 129.6, 126.8, 126.4, 126.2, 123.9, 123.4, 123.1, 123.0, 33.2, 32.0, 31.9, 31.3, 30.8, 30.5, 30.0, 29.8, 29.7, 29.7, 29.6, 29.5, 29.4, 29.4, 29.4, 28.8, 22.7, 22.7, 14.1, 14.1. MALDI-ToF-MS (m/z) calc for $C_{66}H_{86}N_2O_4$ 970.66 found 971.69 $(M+H)^+$ 993.71 $(M+Na)^+$.

N-3,4,5-tridodecylphenyl-N'-methyl-perylene-3,4:9,10-tetracarboxylic acid bisimide **2**

N-3,4,5-tridodecylphenyl-perylene-3,4:9,10-tetracarboxylic acid bisimide (23 mg, 0.024 mmol), K_2CO_3 (98 mg, 0.71 mmol) and MeI (100.2 mg, 0.71 mmol) were charged in dry DMF (3 mL) and stirred overnight under argon atmosphere. The resulting red solution was concentrated in *vacuo* and the residue was subjected to column chromatography with $CHCl_3$:Heptane:MeOH:CH_3COOH/57:48:4:1 as an eluent (R_f = 0.22) to yield the product as a red solid (21 mg, 91% yield). ^{1}H-NMR ($CDCl_3$) δ = 8.61 (d, 2H, PBI), 8.46 (d, 2H, PBI), 8.39 (d, 2H, PBI), 8.31 (d, 2H, PBI), 7.07 (s, 2H, benzylic), 2.66 (t, 6H, CH_2), 1.7-1.2 (mm, 60H, aliphatic), 0.92-0.82 (m, 9H, CH_3). ^{13}C-NMR ($CDCl_3$) δ = 163.2, 163.0, 142.1, 139.2, 133.8, 133.8, 132.2, 131.0, 130.6, 129.2, 128.4, 126.3, 125.7, 125.6, 123.6, 122.8, 122.7, 33.2, 31.9, 31.9, 31.2, 30.8, 30.5, 30.0, 29.8, 29.8, 29.7, 29.7, 29.5, 29.5, 29.4, 29.4, 28.8, 27.1, 22.7, 22.7, 14.1, 14.1. MALDI-ToF-MS (m/z) calc for $C_{67}H_{88}N_2O_4$ 984.67 found 984.67 $(M\cdot)^+$ 1007.66 $(M+Na)^+$.

^{1}H-NMR in $CDCl_3$ (400 MHz) of **1**

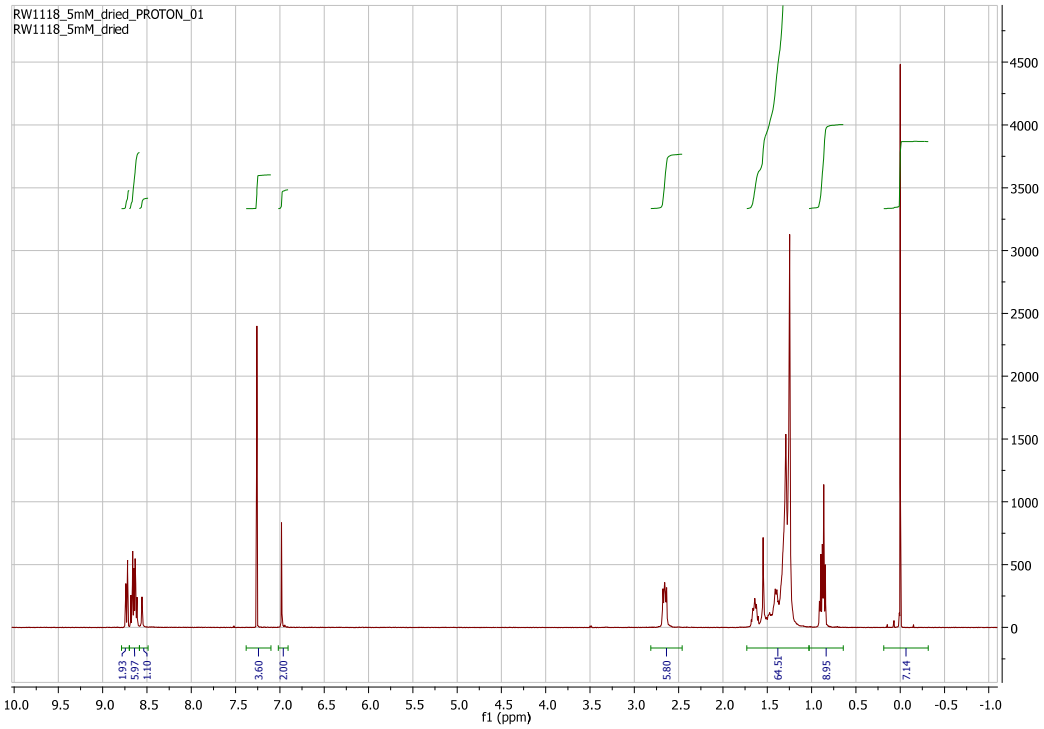

^{13}C-NMR in $CDCl_3$ (100 MHz) of **1**

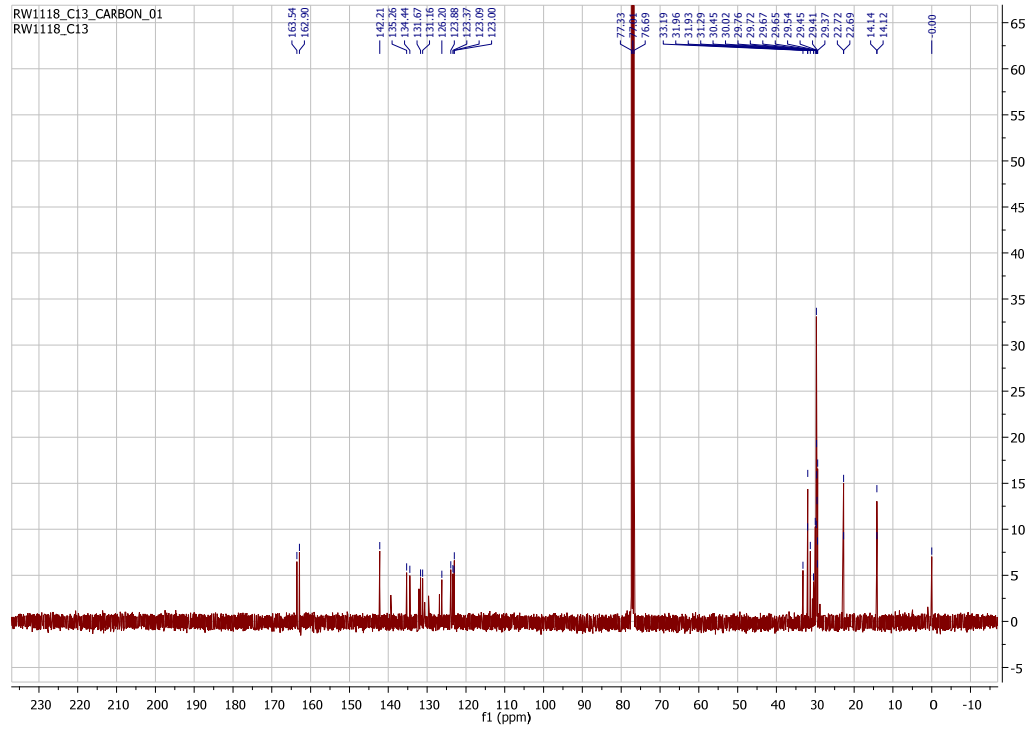

^{1}H-NMR in $CDCl_3$ (400 MHz) of **2**

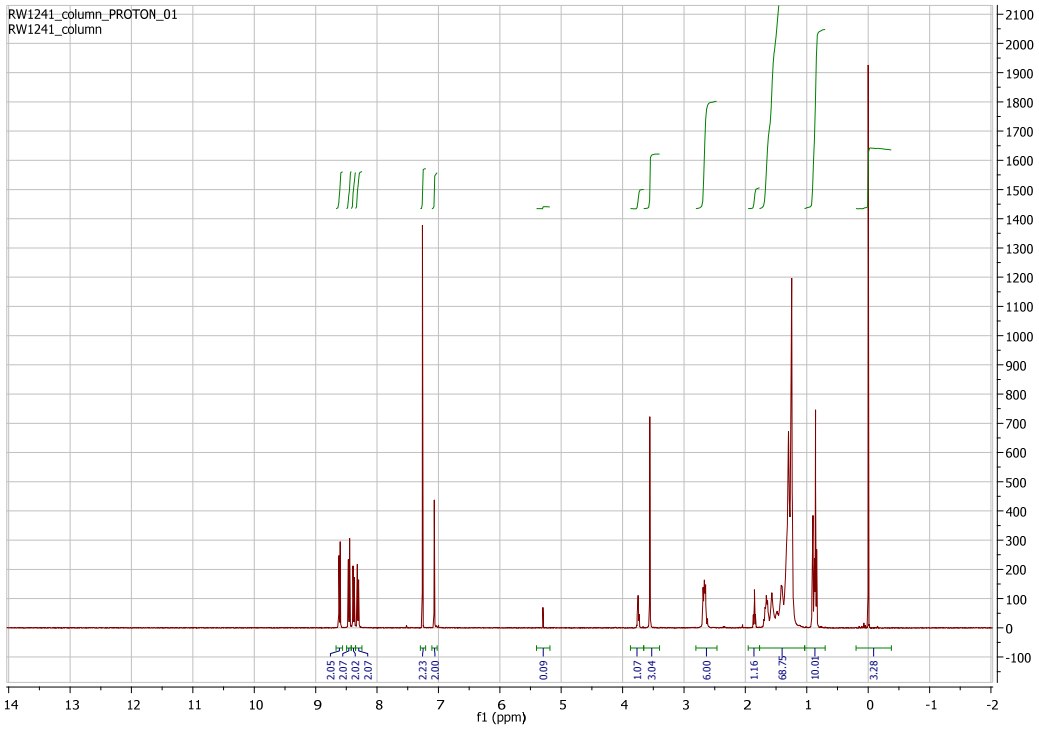

^{13}C-NMR in $CDCl_3$ (100 MHz) of **2**

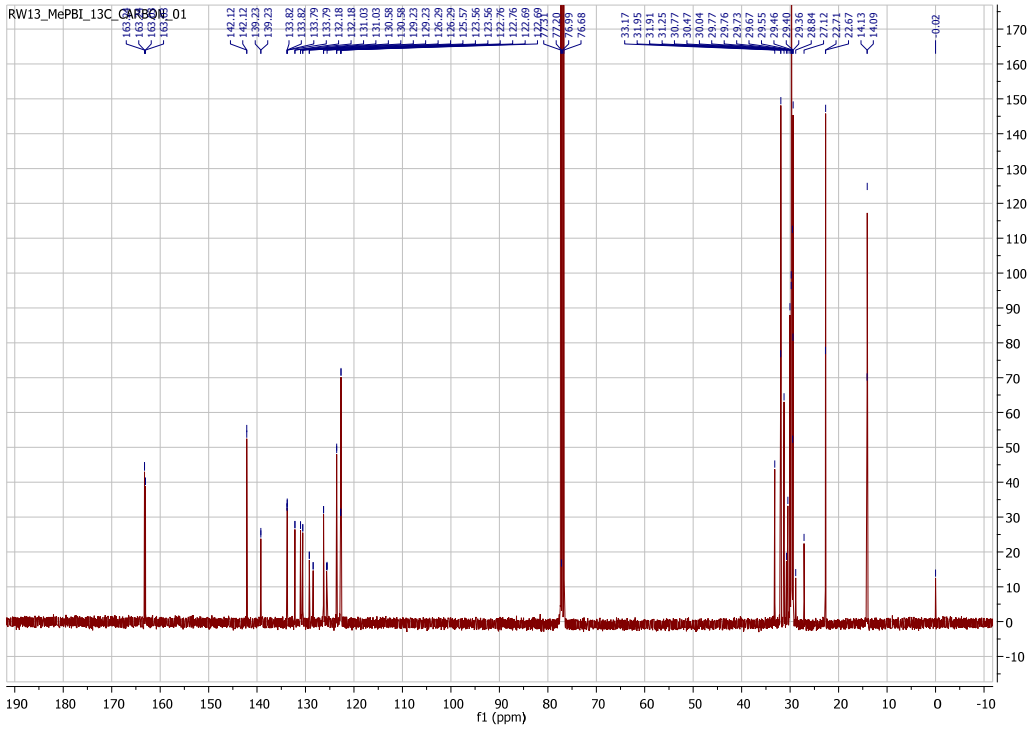

Supporting data

Infrared spectroscopy of PBI 1

The self-assembly of PBI **1** was studied by FT-IR in dilute solution and in solid state. FT-IR spectra in MCH solution (c = 1.10^{-3} M, l = 1 mm, NaCl cell) and in the solid state reveal the same characteristic NH vibration at 3174 cm^{-1} which is strongly indicative of hydrogen bonding (Figure S1 and S2). Furthermore a vibration at 3070 cm^{-1} is observed in both cases and the carbonyl vibrations appear similar at 1670 cm^{-1} and 1702 cm^{-1} (solid state) and 1673 cm^{-1} and 1705 cm^{-1} respectively, indicating similar self-assembly behaviour of PBI **1** in the solid state and MCH solution.

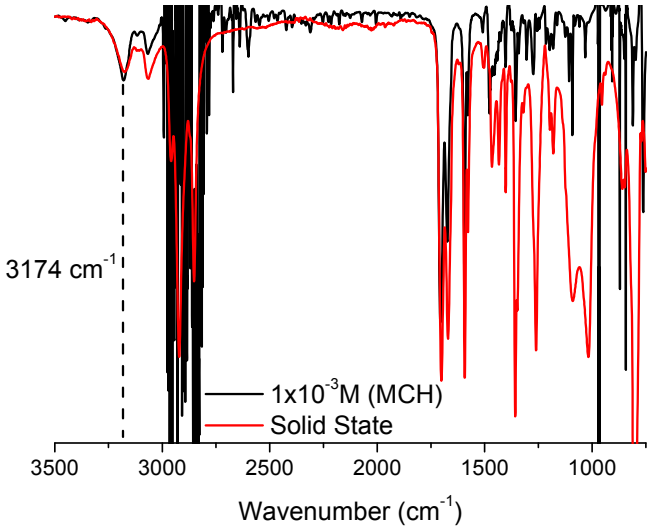

Figure S1: FT-IR spectra for PBI **1** in MCH solution (c = 1.10^{-3} M, l = 1 mm, NaCl cell, T = 20 °C) and solid state.

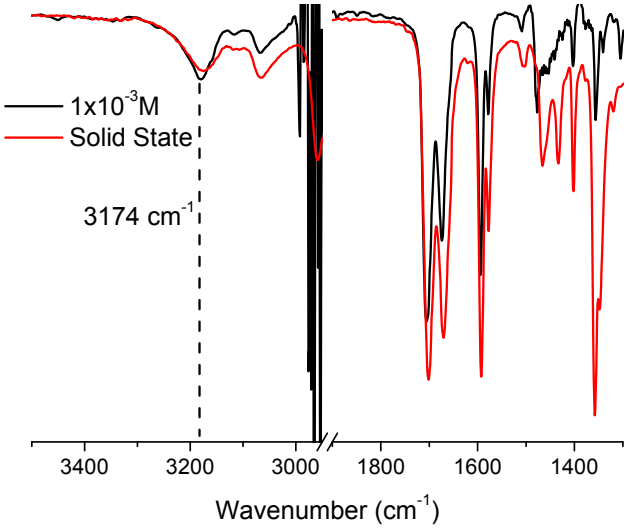

Figure S2: FT-IR spectra for PBI **1** in MCH solution (c = 1.10^{-3} M, l = 1 mm, NaCl cell, T = 20 °C) and solid state. Zoom in on the NH and carbonyl vibration regions.

For reference, FT-IR spectra were also recorded in $CHCl_3$ (c = 1.10^{-3} M) solution, where PBI **1** is molecularly dissolved. Clearly, the NH vibration is shifted to higher wavenumbers (3377 cm^{-1}) with respect to PBI **1** in MCH (Figure S3 and S4). Furthermore slight shifts are observed in the carbonyl region, 1665 cm^{-1} and 1702 cm^{-1} for **1** in $CHCl_3$ compared to 1673 cm^{-1} and 1705 cm^{-1} in MCH respectively. The shifts in the carbonyl region are probably not so visible as multiple different carbonyl fragments are present in PBI **1** that do not all participate in hydrogen bonding.

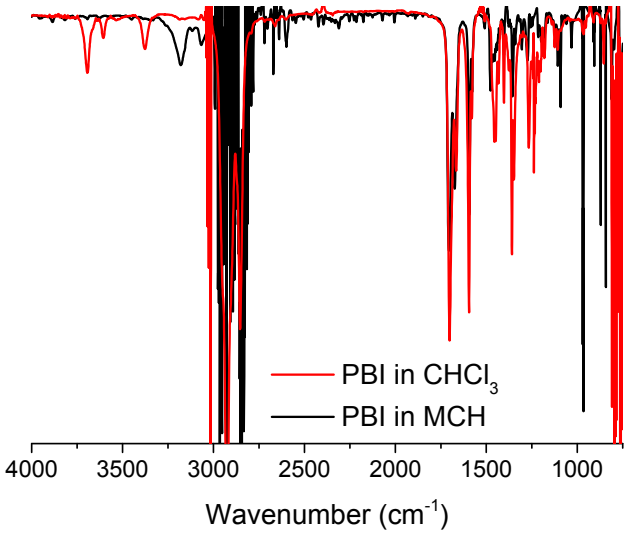

Figure S3: FT-IR spectra for PBI **1** in MCH and $CHCl_3$ solution (c = 1.10^{-3} M, l = 1 mm, NaCl cell, T = 20 °C).

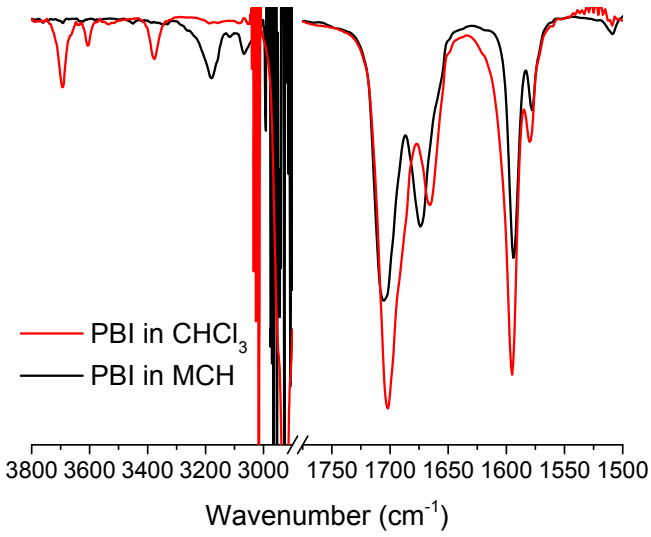

Figure S4: FT-IR spectra for PBI **1** in MCH and $CHCl_3$ solutions (c = 1.10^{-3} M, l = 1 mm, NaCl cell, T = 20 °C). Zoom in on the NH and carbonyl vibration regions.

UV-Vis melting curves of PBI 1

To study the self-assembly mechanism of PBI **1**, UV-Vis cooling curves at various concentrations were recorded (Figure S5).

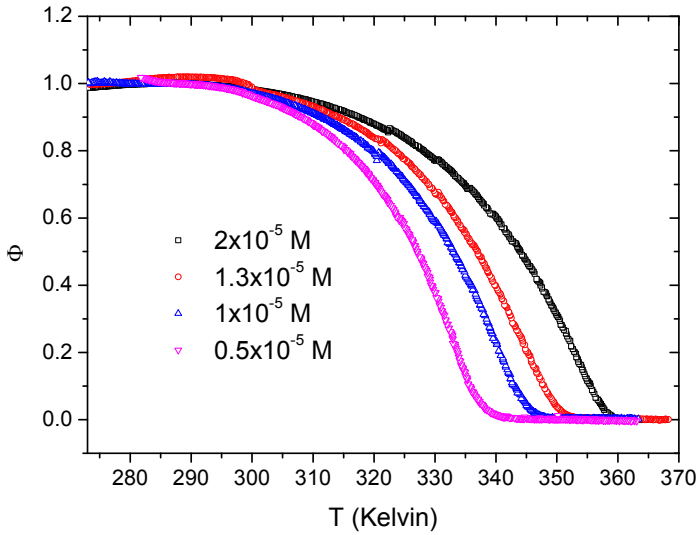

Figure S5: UV-Vis cooling curves measured for PBI **1** at different concentrations (λ = 542 nm, l = 1 cm , MCH, rate = 0.2 °C/min)

SAXS Data analysis of PBI 1

To probe the structure of PBI **1** self-assemblies directly in solution, small angle X-ray scattering experiments were performed at the Swiss light source in Villigen, Switzerland at the cSAXS beamline. SAXS profiles are shown in Figure 2 in the main text and modelled with a form factor describing the scattering of rigid cylinders from which the radius of gyration, R_g, cylinder length L, and the cross section (radius R_{cs}) were obtained (Table S1).,

Table S1: Overview of the SAXS results: radius of gyration, R_g, cylinder length, L / nm, cylinder cross sectional radius, R_{cs} / nm, and the number of perylene bisimide dimers in a stack assuming a π-πdistance of 0.35 nm between subsequent dimers, N_P.

Sample	R_g / nm[a]	L / nm[b]	N_P[b]	R_{cs} / nm[b]	$L/2R_{cs}$[b]	R_g / nm[b]
RW01	1.94±0.03	5.2	30	1.7	1.5	1.9

[a]Obtained from a Guinier approximation ($I(q) = I_0 \exp\left(-\frac{1}{3}R_g^2 q^2\right)$ in the range 0.40 ≤ q ≤ 0.67 nm^{-1}).

[b]Obtained from modelling with a form factor for rigid cylinders using $R_g^2 = \frac{1}{2}R^2 + \frac{1}{12}L^2$.

Self-assembly of N-methylated PBI 2

The self-assembly of PBI **2** in dilute MCH solution was studied with UV-Vis spectroscopy. Similar to PBI **1**, PBI **2** is molecularly dissolved at elevated temperatures (80 °C and c = 2.10^{-4} M) and aggregated at room temperature (Figure S6). The higher stability of aggregates of PBI **1** becomes apparent from the fact that PBI **2** at c = 2.10^{-5} M and 45 °C is still in the molecularly dissolved state while PBI **1** at c = 2.10^{-5} M and 45 °C is almost completely aggregated. A cooling curve measured for PBI **2** (c = 4.10^{-5} M, λ = 540 nm) clearly shows a more sigmoidal behaviour compared to PBI **1** and no critical temperature was observed (Figure S8), indicating the absence of a cooperative self-assembly mechanism for PBI **1**.

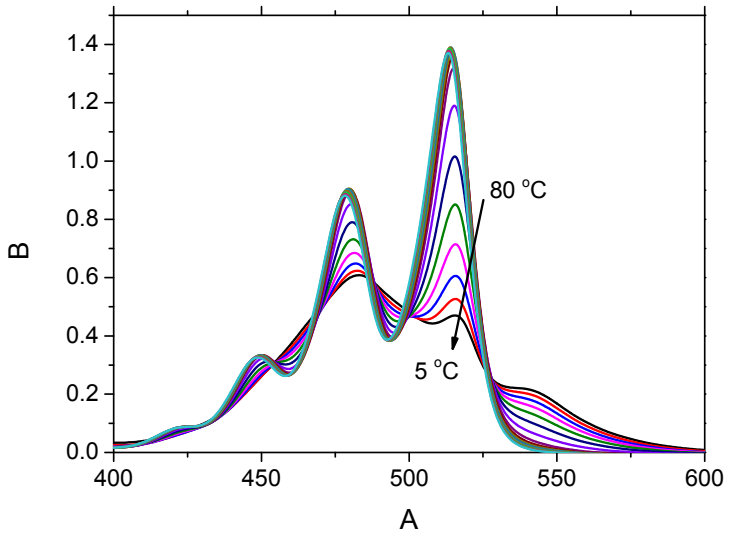

Figure S6: UV-Vis spectra for N-methylated PBI **2** as a function of temperature in MCH (c = 2.10^{-5} M, l = 1 cm, spectrum every five degrees from 80 °C to 5 °C).

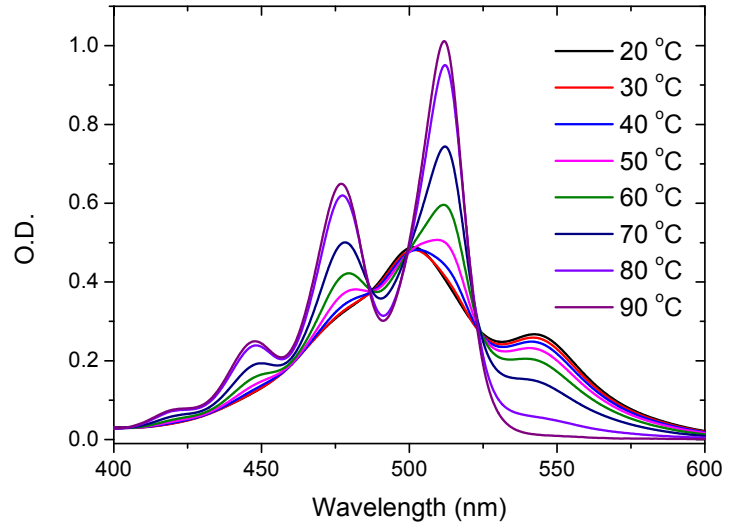

Figure S7: UV-Vis spectra for PBI **1** as a function of temperature in MCH (c = 2.10^{-5} M, l = 1 cm, spectrum every ten degrees from 90 °C to 20 °C).

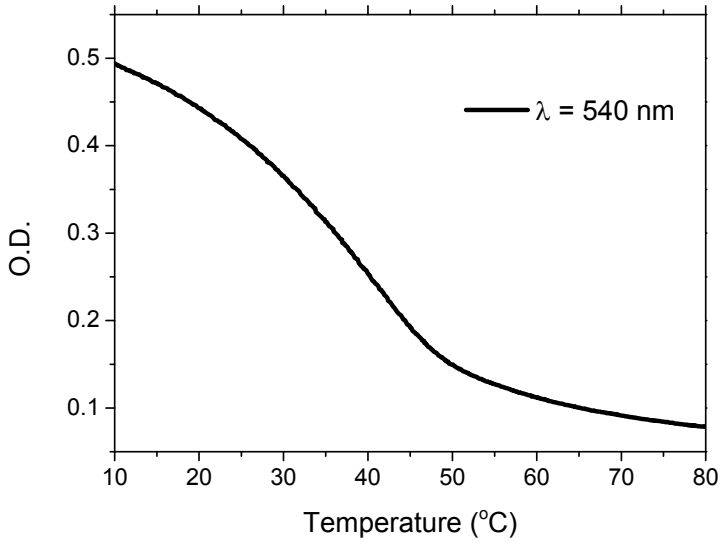

Figure S8: UV-Vis cooling curve of PBI **2** as a function of temperature (λ = 540 nm, c = 4.10^{-5} M, l = 1 cm, rate = 0.2 °C/min).

Thermodynamic modelling of self-assembly of PBI 1

Nucleation-elongation mechanism described with K_2-K equilibrium model

The temperature-dependent assembly of PBI **1** is analysed by using the K_2-K equilibrium model. The model describes the assembly of hydrogen-bonded dimer X as the monomer into one-dimensional assemblies P as a sequence of monomer association and dissociation equilibria. The formation of a nucleus takes place with nucleation equilibrium constant K_2. Monomer addition to the nucleus (with the size of two hydrogen-bonded dimers) and larger species occurs with equilibrium constant of elongation K:

$$\begin{aligned} X + X &\xrightleftharpoons{K_2} P_2 \qquad [P_2] = K_2 [X]^2 \\ P_2 + X &\xrightleftharpoons{K} P_3 \qquad [P_3] = K [P_2][X] \\ &\vdots \\ P_{i-1} + X &\xrightleftharpoons{K} P_i \qquad [P_i] = K [P_{i-1}][X]. \\ &\vdots \end{aligned} \tag{1}$$

The concentration of each species P_i can be expressed as a function of K_2, K and concentration of hydrogen-bonded dimers [X]:

$$[P_2] = K_2 [X]^2, \tag{2}$$

$$[P_i] = K^{i-2} K_2 [X]^i. \tag{3}$$

The equilibrium constants depend on the temperature T via

$$K_2 = \exp\left(-\frac{\Delta H_n^0 - T\Delta S_n^0}{RT} \right), \tag{4}$$

$$K = \exp\left(-\frac{\Delta H_e^0 - T\Delta S_e^0}{RT} \right), \tag{5}$$

where ΔH_n^0 and ΔH_e^0 represent the enthalpy of nucleation and elongation, and ΔS_n^0 and ΔS_e^0 represent the entropy of nucleation and elongation, respectively. Based on these parameters, the degree of aggregation can be calculated as a function of temperature (*vide infra*). However, to increase the accuracy of numerical procedure to solve the mass balance, we define the dimensionless concentration $p_i = K[P_i]$, dimensionless concentration of hydrogen-bonded dimer $x = K[X]$ and cooperativity $\sigma = K_2/K$, and rewrite eq. 2 and 3 in:

$$p_i = \sigma x^i, \qquad \text{for } i \geq 2. \tag{6}$$

The dimensionless mass balance, with $x_{tot} = K \cdot c_{tot}$ (where c_{tot} represents the total concentration of hydrogen-bonded dimers that can be formed, i.e. the total concentration of PBI molecules divided by 2) results in

$$x_{tot} = x + \sigma \sum_{i=2}^{\infty} i x^i. \tag{7}$$

Expanding the sum in eq. 7 yields:

$$x_{tot} = x + \frac{\sigma(2-x)x^2}{(x-1)^2}. \quad (8)$$

Upon solving the dimensionless mass balance by using the *fzero* function in Matlab, x can be found. Subsequently the degree of aggregation φ can be obtained via

$$\varphi = \frac{x_{tot} - x}{x_{tot}}. \quad (9)$$

A global nonlinear least-squares procedure is applied to find the parameters that best describe the temperature-dependent UV-vis data with the equilibrium model. The curve fit, shown in Figure S9A, gives a very good description of the temperature-dependent degree of aggregation. Based on the values of ΔH_n^0, ΔH_e^0, ΔS_n^0 and ΔS_e^0 that are obtained via curve fitting, the temperature-dependent number-averaged degree of polymerization (DP_n) and weight-averaged degree of polymerization (DP_w) can be calculated:

$$DP_n = \frac{\sum_{i=1}^{\infty} iP_i}{\sum_{i=1}^{\infty} P_i} = \frac{x_{tot}}{x + \sigma\sum_{i=2}^{\infty} x^i} = \frac{x_{tot}}{x + \frac{\sigma x^2}{1-x}}, \quad (10)$$

$$DP_w = \frac{\sum_{i=1}^{\infty} i^2 P_i}{\sum_{i=1}^{\infty} iP_i} = \frac{x + \sigma\sum_{i=2}^{\infty} i^2 x^i}{x_{tot}} = \frac{x + \frac{\sigma x^2(4-3x+x^2)}{(x-1)^3}}{x_{tot}}. \quad (11)$$

Alternatively, if the free monomer concentration is not included in the calculation of DP_n and DP_w,

$$DP_n = \frac{\sum_{i=2}^{\infty} iP_i}{\sum_{i=2}^{\infty} P_i} = \frac{x_{tot} - x}{\frac{\sigma x^2}{1-x}}, \quad (12)$$

$$DP_w = \frac{\sum_{i=2}^{\infty} i^2 P_i}{\sum_{i=2}^{\infty} iP_i} = \frac{\frac{\sigma x^2(4-3x+x^2)}{(x-1)^3}}{x_{tot} - x}. \quad (13)$$

As shown in Figure S9B, the temperature-dependent DP_n and DP_w, both with and without the free monomer concentration included in the calculation, suggest the presence of long assemblies in the solution at low temperature. This is in sharp contrast to the observations in SAXS and SLS, and hence a nucleation-elongation mechanism does not apply to the assembly of PBI **1**.

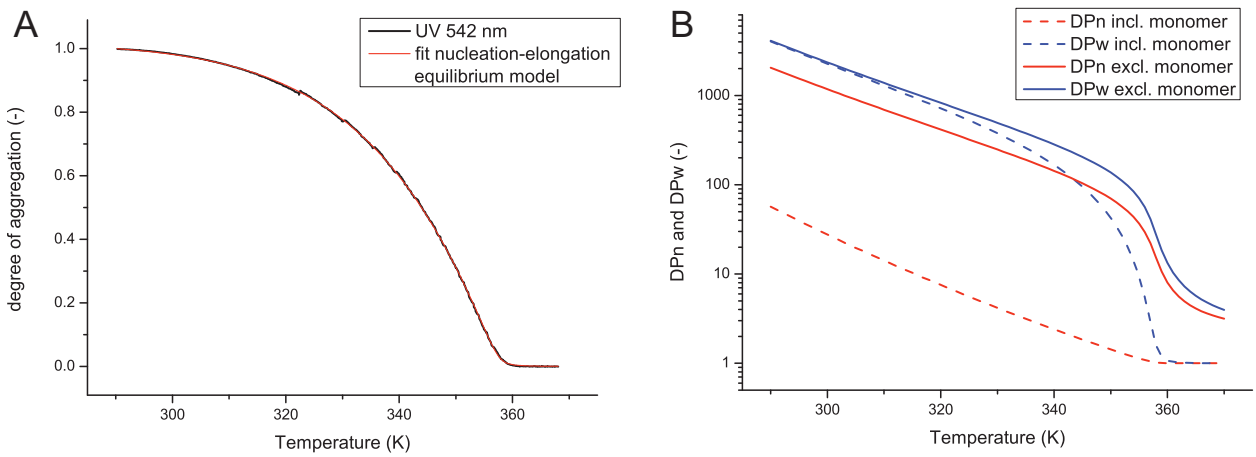

Figure S9: a) Temperature-dependent degree of aggregation of PBI **1**, 20 µM in methylcyclohexane, determined by UV-Vis spectroscopy (542 nm). Curve fitting with the nucleation-elongation K_2-K equilibrium model gives an excellent description of the data. Parameters: ΔH_n^0 = –25.2 ± 0.2 kJ/mol; ΔH_e^0 = –52.22 ± 0.08 kJ/mol; $\Delta S_n^0 = \Delta S_e^0$ = –56.3 ± 0.2 J/K.mol. b) Based on the parameters found via curve fitting in a), the temperature-dependent degrees of polymerization (DP_n, DP_w) are calculated, both inclusive and exclusive the free monomer concentration.

Anti-cooperative mechanism

To analyse if the results can be described with an anti-cooperative growth mechanism which starts with the formation of a dimer that is energetically more favourable compared to further growth by monomer association, *i.e.* $K_2 > K$, simulations using the K_2-K equilibrium model introduced in the previous paragraph are performed with $\sigma = 5$. Although both DP_n and DP_w indicate the formation of small assemblies, the simulated temperature-dependent degree of aggregation does not show a critical temperature of elongation which is experimentally observed (Figure S10). Hence, also an anti-cooperative assembly mechanism does not apply to our molecular system.

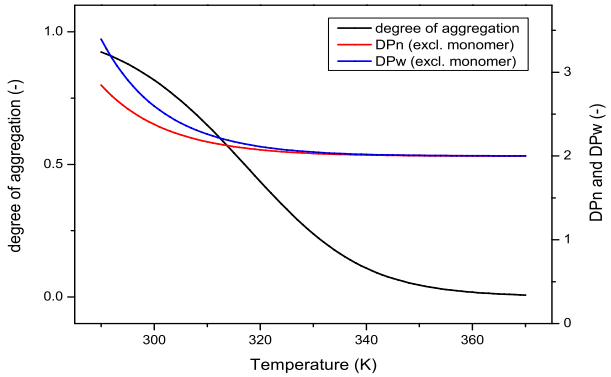

Figure S10: Temperature-dependent degree of aggregation, DP_n and DP_w calculated with anti-cooperative K_2-K equilibrium model. Parameters: ΔH_e = –100 kJ/mol; ΔS_e = –240 J/K.mol; $\sigma = 5$; c_{tot} = 20 µM.

Attenuated growth mechanism

In the attenuated equilibrium model, the equilibrium constant of monomer association K_i depends on the length of the assembly i via $K_i = K/i$:

$$
\begin{aligned}
X + X &\xrightleftharpoons{K_2} P_2 && [P_2] = K_2 [X]^2 = \frac{K}{2}[X]^2 \\
P_2 + X &\xrightleftharpoons{K_3} P_3 && [P_3] = K_3 [P_2][X] = K_3 K_2 [X]^3 = \frac{K}{3}\frac{K}{2}[X]^3 \\
P_3 + X &\xrightleftharpoons{K_4} P_4 && [P_4] = K_4 [P_3][X] = \frac{K}{4}\frac{K}{3}\frac{K}{2}[X]^4 \\
&\vdots \\
P_{i-1} + X &\xrightleftharpoons{K_i} P_i && [P_i] = K_i [P_{i-1}][X] = \frac{K}{i}\frac{K}{i-1}\cdots\frac{K}{3}\frac{K}{2}[X]^i = \frac{K^{i-1}}{i!}[X]^i .
\end{aligned}
\qquad (14)
$$

Again, monomer X represents the hydrogen-bonded dimer. The resulting mass balance is

$$c_{tot} = X + \sum_{i=2}^{\infty} i \frac{K^{i-1}}{i!}[X]^i , \qquad (15)$$

analogously the dimensionless mass balance, with $x_{tot} = K \cdot c_{tot}$ and $x = K \cdot [X]$, is

$$x_{tot} = x + \sum_{i=2}^{\infty} i \frac{x^i}{i!} . \qquad (16)$$

Expanding the sum in eq. 16 yields:

$$x_{tot} = x + x\left(e^x - 1\right) = xe^x . \qquad (17)$$

By solving the mass balance using a numerical method, the dimensionless monomer concentration x can be found, and subsequently DP_n and DP_w (excluding the contribution from the monomers) can be calculated:

$$DP_n = \frac{\sum_{i=2}^{\infty} iP_i}{\sum_{i=2}^{\infty} P_i} = \frac{x_{tot} - x}{\sum_{i=2}^{\infty} \frac{x^i}{i!}} = \frac{x_{tot} - x}{e^x - x - 1} , \qquad (18)$$

$$DP_w = \frac{\sum_{i=2}^{\infty} i^2 P_i}{\sum_{i=2}^{\infty} iP_i} = \frac{\sum_{i=2}^{\infty} i^2 \frac{x^i}{i!}}{x_{tot} - x} = \frac{e^x\left(x + x^2\right) - x}{x_{tot} - x} . \qquad (19)$$

In contrast to previous simulations, here we analyse the degree of aggregation as well as DP_n and DP_w as a function of dimensionless concentration x_{tot} instead of temperature. Since $x_{tot} = K \cdot c_{tot}$, the dimensionless concentration can be increased by both increasing the concentration as well as decreasing the temperature.

Although the attenuated equilibrium model predicts small values for DP_n and DP_w, the resulting degree of aggregation does not include a critical point which marks the onset of aggregation (Figure S11A). This is in contrast to the experimental results, and hence this model cannot describe the assembly of PBI **1**.

In an attempt to introduce a critical point at which the aggregation process starts, we include an energetically unfavourable nucleation in the attenuated equilibrium model, *i.e.* $K_2 = \sigma \cdot K/2$ with $\sigma < 1$:

$$\begin{aligned} X + X &\xrightleftharpoons{K_2} P_2 \qquad [P_2] = K_2 [X]^2 = \sigma \frac{K}{2} [X]^2 \\ &\vdots \\ P_{i-1} + X &\xrightleftharpoons{K_i} P_i \qquad [P_i] = K_i [P_{i-1}][X] = \sigma \frac{K}{i} \frac{K}{i-1} \cdots \frac{K}{3} \frac{K}{2} [X]^i = \sigma \frac{K^{i-1}}{i!} [X]^i . \\ &\vdots \end{aligned} \tag{20}$$

The resulting equations for the mass balance, DP_n and DP_w become:

$$x_{tot} = x + \sigma x \left(e^x - 1 \right) \tag{21}$$

$$DP_n = \frac{\sum_{i=2}^{\infty} i P_i}{\sum_{i=2}^{\infty} P_i} = \frac{x_{tot} - x}{\sigma \left(e^x - x - 1 \right)}, \tag{22}$$

$$DP_w = \frac{\sum_{i=2}^{\infty} i^2 P_i}{\sum_{i=2}^{\infty} i P_i} = \frac{\sigma \left(e^x \left(x + x^2 \right) - x \right)}{x_{tot} - x}. \tag{23}$$

As shown in Figure S11B, the attenuated equilibrium model that includes an unfavourable nucleation (σ = 0.001) predicts both a critical point as well as the formation of short assemblies, even at very high values of x_{tot}.

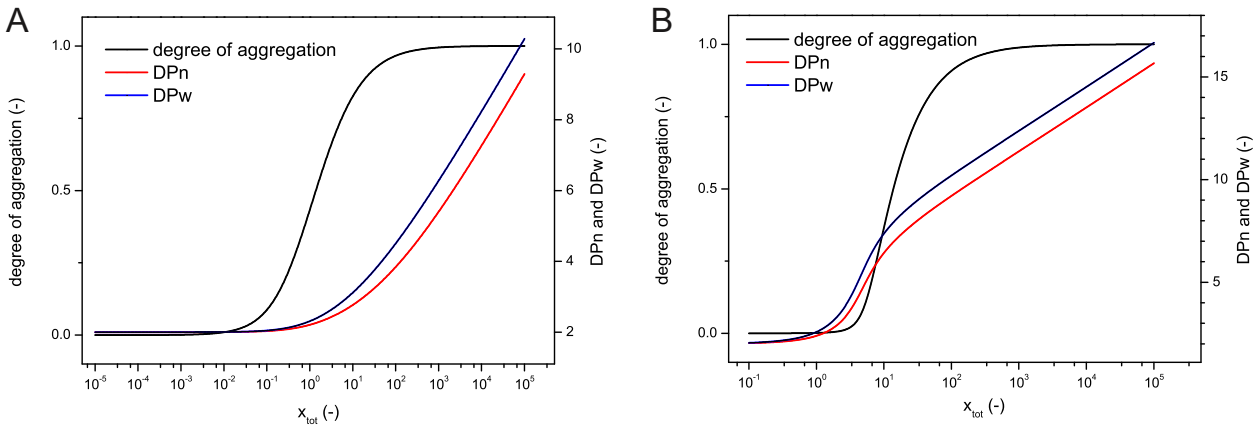

Figure S11: Degree of aggregation, DP_n and DP_w *vs*. dimensionless total concentration x_{tot}, simulated with attenuated equilibrium model. With σ = 1 (a) no critical point is observed, however with σ = 0.001 (b) a critical point marks the onset of aggregation whereas DP_n and DP_w are–even at high x_{tot}–small.

Attenuated growth preceded by unfavourable formation of a hydrogen-bonded dimer

To analyse if the critical temperature that is observed in the temperature-dependent assembly together with the formation of short assemblies can also be described by the attenuated assembly of hydrogen-bonded dimers, we modify the model that is introduced in the previous section. Initially, two PBI molecules *A* combine to form a hydrogen-bonded dimer *X*, with equilibrium constant K_h. Subsequently, the hydrogen-bonded dimers assemble via stepwise association equilibria into assemblies *P*. The equilibrium constants involved in these association equilibria K_i again depend on the length of the assembly via $K_i = K/i$:

$$
\begin{aligned}
&A + A \overset{K_h}{\rightleftarrows} X && [X] = K_h [A]^2 \\
&X + X \overset{K_2}{\rightleftarrows} P_2 && [P_2] = K_2 [X]^2 = \frac{K}{2} K_h^2 [A]^4 \\
&P_2 + X \overset{K_3}{\rightleftarrows} P_3 && [P_3] = K_3 [P_2][X] = K_3 K_2 [X]^3 = \frac{K}{3}\frac{K}{2} K_h^3 [A]^6 \\
&P_3 + X \overset{K_4}{\rightleftarrows} P_4 && [P_4] = K_4 [P_3][X] = \frac{K}{4}\frac{K}{3}\frac{K}{2} K_h^4 [A]^8 \\
&\quad\vdots \\
&P_{i-1} + X \overset{K_i}{\rightleftarrows} P_i && [P_i] = K_i [P_{i-1}][X] = \frac{K}{i}\frac{K}{i-1}\cdots\frac{K}{3}\frac{K}{2}[X]^i = \frac{K^{i-1}}{i!} K_h^i [A]^{2i}. \\
&\quad\vdots
\end{aligned}
\tag{24}
$$

The resulting mass balance is

$$
c_{tot} = A + 2X + 2\sum_{i=2}^{\infty} iP_i = A + 2K_h [A]^2 + 2\sum_{i=2}^{\infty} i \frac{K^{i-1}}{i!} K_h^i [A]^{2i}, \tag{25}
$$

where c_{tot} represents the total concentration of PBI. Analogously the dimensionless mass balance, with $\alpha = K_h / K$, $x_{tot} = K \cdot c_{tot}$ and $x = K \cdot [A]$:

$$
x_{tot} = x + 2\alpha x^2 + 2\sum_{i=2}^{\infty} i \frac{(\alpha x^2)^i}{i!}. \tag{26}
$$

Expanding the sum in eq. 26 yields:

$$
x_{tot} = x + 2\alpha x^2 + 2\alpha x^2 \left(e^{\alpha x^2} - 1\right) = x + 2\alpha x^2 e^{\alpha x^2}. \tag{27}
$$

Upon numerically solving the mass balance, the dimensionless PBI concentration *x* can be found. Subsequently, DP_n and DP_w are calculated, based on the material that is present in the assemblies P_i, with $i \geq 2$:

$$
DP_n = \frac{\sum_{i=2}^{\infty} iP_i}{\sum_{i=2}^{\infty} P_i} = \frac{x_{tot} - x - 2\alpha x^2}{\sum_{i=2}^{\infty} \frac{(\alpha x^2)^i}{i!}} = \frac{x_{tot} - x - 2\alpha x^2}{e^{\alpha x^2} - \alpha x^2 - 1}, \tag{28}
$$

$$DP_{\mathrm{w}} = \frac{\sum_{\mathrm{i}=2}^{\infty} i^2 P_{\mathrm{i}}}{\sum_{\mathrm{i}=2}^{\infty} i P_{\mathrm{i}}} = \frac{\sum_{\mathrm{i}=2}^{\infty} (2i)^2 \frac{(\alpha x^2)^{\mathrm{i}}}{i!}}{x_{\mathrm{tot}} - x - 2\alpha x^2} = \frac{4\left(\mathrm{e}^{\alpha x^2}\left(\alpha x^2 + \alpha^2 x^4\right) - \alpha x^2\right)}{x_{\mathrm{tot}} - x - 2\alpha x^2}. \quad (29)$$

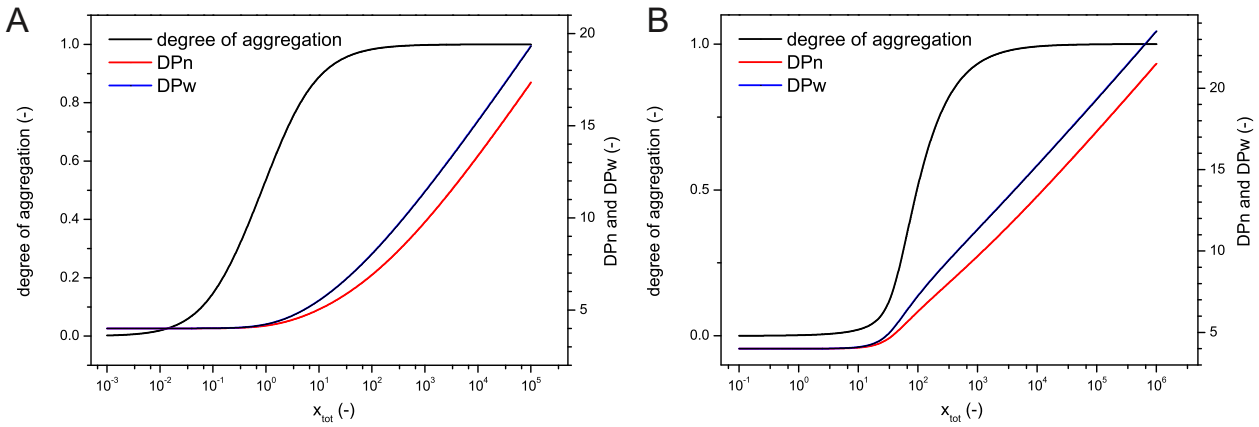

Figure S12: Degree of aggregation, DP_{n} and DP_{w} *vs*. dimensionless total concentration x_{tot}, simulated with attenuated equilibrium model preceded by the formation of a hydrogen-bonded dimer. With α = 1 (a) no critical point is observed, however with α = 0.001 (b) a critical point marks the onset of aggregation whereas DP_{n} and DP_{w} are–even at high x_{tot}–small.

References

1 P. Lindner and T. Zemb, eds., *Neutron, X-rays and Light: Scattering Methods Applied to Soft Condensed Matter* Elsevier, Amsterdam, 2002

2 H. Kaiser, J. Lindner, H. Langhals, *Chem. Ber.*, 1991, **124**, 529

3 X. Zhang, Z. Chen, F. Würthner, *J. Am. Chem. Soc.*, 2007, **129**, 4886

4 Z. Chen, V. Stepanenko, V. Dehm, P. Prins, L.D.A. Siebbeles, J. Seibt, P. Marquetand, V. Engel, F. Würthner, *Chem. Eur. J.*, 2007, **13**, 436